Activation of Individual αIIbβ3 Integrin Molecules by Disruption of Transmembrane Domain Interactions in the Absence of Clustering†

Rustem I. Litvinov,‡ Gaston Vilaire,§ Wei Li,§ William F. DeGrado,|| John W. Weisel,‡ and Joel S. Bennett*,§

Department of Cell and Developmental Biology, Department of Biochemistry and Biophysics, and Hematology−Oncology Division of the Department of Medicine, University of Pennsylvania School of Medicine, Philadelphia, Pennsylvania 19104

Received December 30, 2005; Revised Manuscript Received March 3, 2006

ABSTRACT: We used laser tweezers-based force spectroscopy to measure the binding strength between fibrinogen molecules covalently bound to latex beads and either wild-type αIIbβ3 molecules or αIIbβ3 molecules containing the transmembrane domain mutations β3 G708N or αIIb G972N expressed on Chinese hamster ovary cells. As we demonstrated previously for αIIbβ3 on agonist-stimulated platelets and for purified αIIbβ3 molecules incubated with Mn^{2+}, two regimes of rupture forces were present when wild-type αIIbβ3 was activated by the monoclonal antibody PT25-2: rupture forces of 20−60 pN with an exponentially decreasing probability of detection and rupture forces in the range of 60−150 pN with a maximum at ∼70−80 pN. Both rupture force regimes were specific for fibrinogen binding to the activated conformation of αIIbβ3 because they were inhibited by αIIbβ3-specific antagonists. Identical rupture force regimes were present constitutively when cells expressing the αIIb and β3 transmembrane domain mutants were studied, confirming that these mutations induced an active αIIbβ3 conformation. Moreover, there were no significant differences in the yield strength of the low-to-moderate and strong force regimes when αIIbβ3 was activated by PT25-2 or the transmembrane domain mutations, implying that there was no fundamental difference in the way these forms of activated αIIbβ3 interacted with fibrinogen. Thus, the two-step pathway of the interaction of αIIbβ3 with fibrinogen we have identified appears to be a fundamental property of the high-affinity state of αIIbβ3 and is identical regardless of whether this affinity state is achieved by intracellular, extracellular, or membrane-associated events.

Integrins are ubiquitous cell adhesion molecules that mediate cell−matrix and cell−cell interactions by binding to specific macromolecular protein ligands. The ability of integrins to bind ligands can be regulated by intracellular reactions, a process termed "inside-out" signaling. Conversely, ligand-occupied integrins, via "outside-in" signaling, regulate intracellular activity and processes such as cell motility, spreading, and proliferation. Integrins are noncovalent α/β heterodimers, each subunit consisting of a large extracellular headpiece, a transmembrane (TM)[1] helix, and a short cytoplasmic tail (*1*−*3*). The behavior of the major platelet integrin αIIbβ3 represents the prototypic example of integrin regulation. αIIbβ3 mediates platelet aggregation when agonists induce fibrinogen and/or von Willebrand factor binding to its extracellular headpiece. However, because fibrinogen and von Willebrand factor are normal constituents of blood, ligand binding to αIIbβ3 is tightly regulated to prevent the formation of unwanted and potentially harmful intravascular platelet aggregates. Thus, αIIbβ3 is inactive on unstimulated platelets and active following platelet stimulation.

αIIbβ3 resides on the platelet surface in an equilibrium between low-affinity and high-affinity conformations that can be shifted in either direction by stabilizing one conformation over the other (*4*). The shift from a low-affinity to a high-affinity conformation results from a rearrangement of the entire αIIbβ3 molecule that includes separation of its TM and cytoplasmic domains, which are in proximity in the low-affinity state (*5*). Separation of the TM domains is an essential feature of this rearrangement (*6*) and likely contributes to the αIIbβ3 clustering that is observed coincident with or following ligand binding (*7*, *8*).

The TM helices of αIIb and β3 can undergo homomeric association in micelles (*9*) and in bacterial membrane bilayers (*10*). We reported previously that mutations in the β3 TM domain that enhance its homomeric association in micelles and bacterial membranes also induce αIIbβ3 activation and clustering (*8*). Similarly, mutations in the αIIb TM helix that disrupt its homomeric association also induce αIIbβ3 activation and clustering (*11*). These observations suggest a "push−pull" mechanism for αIIbβ3 regulation in which disruption of interactions involving the αIIb TM helix, most likely its heteromeric interaction with the β3 TM helix (*12*), pushes αIIbβ3 to a high-affinity conformation and subsequent

† This work was supported by grants from the National Institutes of Health, HL40387 (to J.S.B.) and HL30954 (to J.W.W.).

* Corresponding author. Tel: 215-573-3280. Fax: 215-573-7039. E-mail: bennetts@mail.med.upenn.edu.

‡ Department of Cell and Developmental Biology, University of Pennsylvania School of Medicine.

§ Hematology−Oncology Division of the Department of Medicine, University of Pennsylvania School of Medicine.

|| Department of Biochemistry and Biophysics, University of Pennsylvania School of Medicine.

[1] Abbreviations: TM, transmembrane; mAb, monoclonal antibody; CHO, Chinese hamster ovary; WT, wild type; FACS, fluorescence-activated cell sorting; MES, 2-(*N*-morpholino)ethanesulfonic acid; BSA, bovine serum albumin; cRGD, cyclic Arg-Gly-Asp peptide.

10.1021/bi0526581 CCC: $33.50
Published on Web 03/28/2006

homomeric αIIb and β3 interactions pull it to a stable high-affinity and clustered state (*11*). However, whether disrupting the association of the αIIb and β3 TM helices is sufficient to shift αIIbβ3 to its high-affinity state and whether αIIbβ3 clustering participates in the equilibrium between its low- and high-affinity conformations remain controversial (*13*).

One way to address these questions is to study the consequences of TM helix mutations at the single-molecule level using laser tweezer-based force spectroscopy. Laser tweezers are an optical system in which external forces applied to a spherical particle trapped by a focused laser beam can be accurately measured because the displacement of the trapped bead is directly proportional to the lateral force applied to the particle. Laser tweezers are sensitive and accurate at the lower end of the force spectrum (0−200 pN) (*14*); thus, they are a suitable system with which to measure the force of interaction between individual receptor−ligand pairs (*15*). Previously, we used laser tweezers to measure rupture forces between fibrinogen and αIIbβ3 on platelets (*16*). We found that the forced unbinding of fibrinogen from αIIbβ3 is a complex, time-dependent, multistep process with at least two force regimes: a low-to-moderate regime with rupture forces in the range of 20−60 pN and strong regime with rupture forces ranging from 60 to 150 pN and a maximum at 80−100 pN (*16*, *17*).

Here we used laser tweezers to compare the fibrinogen-binding strength of individual wild-type (WT) αIIbβ3 molecules activated by a "LIBS" monoclonal antibody (mAb) to αIIbβ3 molecules containing either of the TM helix mutations β3 G708N and αIIb G972N (*8*, *10*, *11*). We found that both mutations resulted in the expression of constitutively active αIIbβ3 molecules that bound fibrinogen with the same strength as mAb-activated WT αIIbβ3. Thus, these experiments directly demonstrate that perturbing TM helix interactions are sufficient by themselves to induce the high-affinity conformation of single αIIbβ3 molecules.

MATERIALS AND METHODS

Stable Expression of αIIbβ3 in Chinese Hamster Ovary (CHO) Cells. CHO cells were cultured in Ham's F-12 medium (Life Technologies, Inc., Gaithersburg, MD) supplemented with 10% fetal bovine serum (HyClone Laboratories Inc., Logan, UT). cDNAs encoding WT or mutated human β3 and αIIb were subcloned into pcDNA3.1(+)-Zeo and pcDNA3.1(+)-Neo, respectively. Mutant αIIb or mutant β3 and the complementary WT subunit were then cotransfected into CHO cells using FUGENE 6 (Roche Diagnostics Corp., Indianapolis, IN). Two days after transfection, the cells were transferred to selection medium containing 500 mg/mL G418 (Life Technologies, Inc., Gaithersburg, MD) and 300 mg/mL Zeocin (Invitrogen, Carlsbad, CA). After 3 weeks, cells were sorted by fluorescence-activated cell sorting (FACS) to obtain cell lines expressing high levels of αIIbβ3. Subsequent experiments using the sorted cells were conducted at room temperature within 4 h of placing the cells in suspension.

Preparation of Fibrinogen-Coated Beads. Human fibrinogen (American Diagnostica, Inc., Stamford, CT) was covalently bound to 0.93 μm carboxylate-modified latex beads (Bangs Laboratories, Inc., Fishers, IN) using *N*-(3-dimethylaminopropyl)-*N*′-ethylcarbodiimide hydrochloride (Sigma, St. Louis, MO) as a cross-linking agent in a two-step procedure. After activation of the bead surface in 0.1 M MES, pH 5.2, by mixing 1 mL of the buffer, 10 μL of a 10% bead suspension, and 1.5 mg of dry carbodiimide, followed by constant shaking for 15 min at 4 °C, the beads were sedimented (4250*g*, 2 min), washed once with binding buffer (0.055 M borate buffer, pH 8.5), resedimented, and suspended in 20 μg/mL fibrinogen solution in binding buffer. After 15 min incubation with stirring at 4 °C, the beads were sedimented and resuspended in BSA solution (2 mg/mL in 0.055 M borate buffer, pH 8.5) or 1 M ethanolamine solution in the same buffer. The surface density of fibrinogen, determined using ^{125}I-labeled protein, was near the saturation point of $(11 \pm 2) \times 10^{-9}$ μg/μm^2. Fibrinogen-coated beads were freshly prepared and mildly sonicated to disrupt aggregates before each experiment.

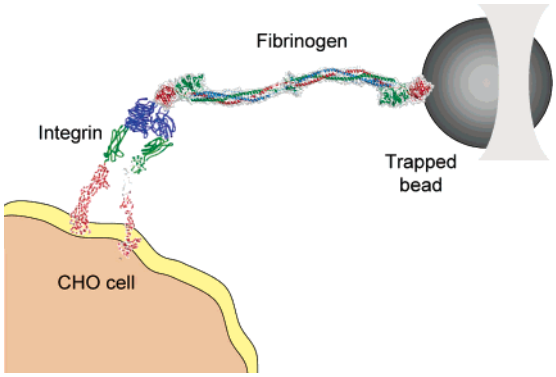

FIGURE 1: Schematic representation of the bimolecular interaction between the integrin αIIbβ3 expressed by a CHO cell and fibrinogen bound covalently to a trapped latex bead. The cartoon is based on crystallographic (*3*) and electron microscope (*5*) data and approximates the relative positions and dimensions of the interacting molecules. The central part of the fibrinogen molecule, comprising the N-terminal portions of its constituent polypeptide chains, is highly flexible and has not been visualized in the crystal structure.

Laser Tweezer-Based Measurement of the αIIbβ3−Fibrinogen Interactions (Figure 1). A mixture of CHO cells and fibrinogen-coated beads (~10^6/mL each), suspended in culture medium with or without the αIIbβ3-activating mAb PT25-2 (*18*), was placed in a flow chamber. After the chamber was placed on a microscope stage, the cells were allowed to settle onto the polylysine-coated bottom of the chamber for 5−10 min. Using a manual stage, an adherent CHO cell was selected and brought to the center of the microscopic field. A fibrinogen-coated bead in the vicinity of the cell was then trapped by the laser beam, and the microscope focus was adjusted so that the bead and cell centers were approximately the same distance from the surface of the bottom. The position of the laser trap, and hence the position of the bead, was then oscillated in the *x*-direction in a triangular waveform at a frequency of 50 Hz and at a constant peak-to-peak amplitude of 0.8 μm. At a trap stiffness of 0.2 pN/nm, this results in a loading rate of 16000 pN/s. The separation of the cell and the bead was then reduced in 10 nm steps with a piezostage until repeated contacts between the bead and cell were observed. When the CHO cell and the fibrinogen-coated bead bound, force was exerted by the trap on the bead during their separation. If the force was sufficient to detach the bead from the cell membrane, it was registered as the rupture force and reflected the bond strength between the bead and the cell surface. The

laser tweezer setup and the bead position sensing system have been described elsewhere in detail (*16*, *17*).

Data Processing and Analysis. Data were recorded and analyzed with custom LabVIEW (National Instruments, Austin, TX) software. The position of a trapped bead and its displacement from the laser beam focus were recorded with 0.5 ms time resolution as a digitized voltage curve consisting of many individual voltage (force) signals each reflecting a binding/rupture event (*16*, *17*). The LabVIEW-based software recognized the peak, calculated the amplitude of each signal, and presented each peak in force units based on a calibration coefficient. To obtain reasonable statistics, rupture force measurements were made at a high repetition rate. Rupture forces from interactions between $>10^3$ cell−bead pairs were collected and displayed as force histograms for different experimental conditions. The sequence of rupture forces was sorted into a histogram with 10 pN wide bins and normalized by the total number of contacts. The percentage of events in a particular force range (bin) represents the probability of a bond rupture in that force range. As inferred from numerous controls, forces in the range of 0−10 pN, the first bin in the histograms, represent noise or optical artifacts in combination with weak nonspecific interactions (*16*, *17*). Accordingly, the first bin could be neglected without affecting the results since meaningful events only occurred within the force range of 20−150 pN. The results of experiments for multiple (∼20−90) cell−bead pairs under similar experimental conditions were averaged so that each force histogram represented about 10^4-10^5 contacts between similar reacting surfaces.

Because a typical histogram of rupture forces contained regimes of low-to-moderate (20−60 pN) and strong (>60 pN) binding, the two components of the histogram were modeled with empirically determined function as the sum of an exponential and a Gaussian curve as described by eq 1 (*17*).

$$Y = a_1 \exp(-x/b_1) + a_2 \exp(-((x - c)/b_2)^\wedge 2) \quad (1)$$

This two-component fit was used to quantify the force distributions and to compare αIIbβ3−fibrinogen interactions registered under different experimental conditions (Figures 3−5 and Tables 1−3). The yield forces in the range of 20−60 pN were typically well fit with an exponential, and stronger forces in the range of 60−150 pN were well fit with a Gaussian curve centered at ∼70−80 pN. The fit parameter b_1 gives the average and c gives the most probable rupture forces (yield strength) for the low-to-moderate and strong interactions, respectively.

RESULTS

Interaction of Fibrinogen with CHO Cells Expressing WT αIIbβ3 Integrin. To determine the baseline adhesiveness of CHO cells in our laser tweezer model system and to distinguish between specific receptor−ligand and nonspecific cell−protein interactions, we performed two types of experiments. First, we measured the interaction of CHO cells expressing WT αIIbβ3 in its low-affinity state with BSA- and fibrinogen-coated beads. When beads were coated with BSA, the vast majority of measured rupture forces were in the range of 0−20 pN with an exponentially decreasing probability of detecting greater forces. Thus, the cumulative probability of detecting rupture forces >20 pN was only 0.12% (Figure 2A). The CHO cells were slightly more reactive when beads were coated with fibrinogen, such that the cumulative probability of detecting rupture forces >20 pN was 0.7% (Figure 2B). Second, we studied CHO cells expressing WT αIIbβ3 that had been shifted to its high-affinity state by the mAb PT25-2. In the presence of PT25-2, there was a substantial difference in the interaction of the cells with BSA- and fibrinogen-coated beads. When beads were coated with BSA, the large majority of the interactions remained below 20 pN, and the cumulative probability of measuring forces >20 pN was 0.9%, comparable to that of cells expressing low-affinity αIIbβ3. Moreover, the force profile decreased exponentially (Figure 2C), typical for nonspecific protein−cell interactions (*16*). By contrast, when beads were coated with fibrinogen, the cumulative probability of measuring forces >20 pN increased significantly to 3.9%, and the histogram of rupture forces displayed two force regimes: a low-to-moderate regime with forces in the range of 20−60 pN and a strong regime of forces >60 pN, the pattern observed for the interaction of fibrinogen with the high-affinity conformation of αIIbβ3 on platelets (Figure 2D) (*16*).

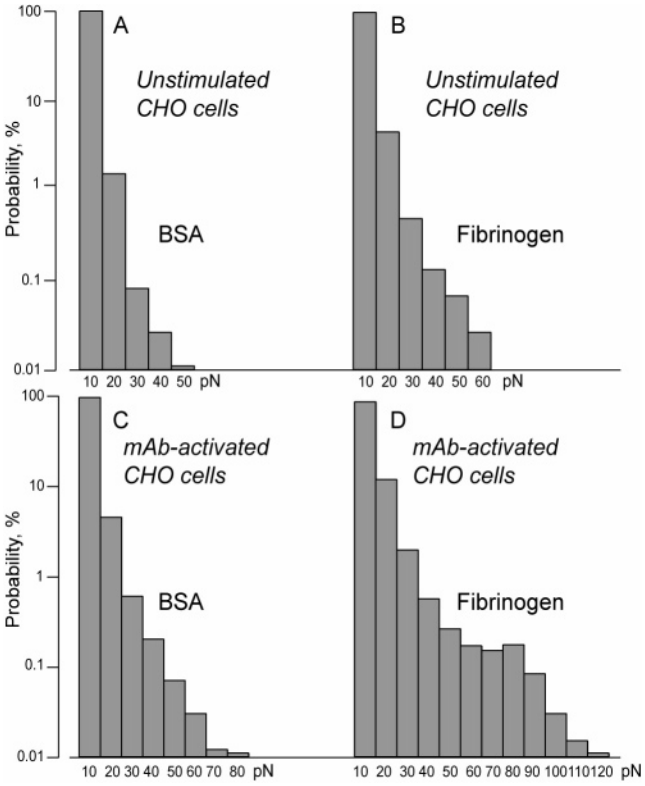

FIGURE 2: Rupture force histograms of the interactions of unstimulated (A, B) and mAb PT25-2-activated (B, C) CHO cells expressing WT αIIbβ3 with BSA-coated (A, C) versus fibrinogen-coated (B, D) beads. The activated cells were pretreated with 100 μg/mL mAb PT25-2 for 15 min at 37 °C. The rupture forces were arranged into histograms with 10 pN wide bins and normalized by the total number of counts (n) for each experimental condition [n = 22 850 for (A), n = 14 564 for (B), n = 53 950 for (C), and n = 140 496 for (D)].

To confirm that rupture forces >20 pN induced by PT25-2 represented specific fibrinogen binding to αIIbβ3, we measured the effect of well-characterized αIIbβ3 antagonists: the H12 peptide derived from the carboxyl terminus of the fibrinogen γ-chain (*19*); the αIIbβ3-specific mAb

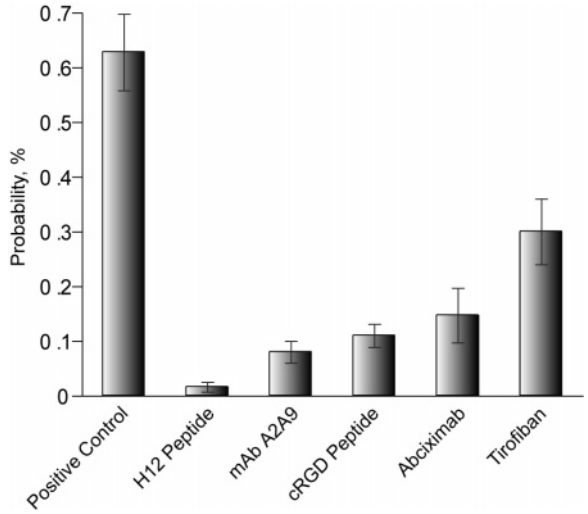

FIGURE 3: Probability of interactions producing rupture forces >20 pN between fibrinogen and the WT αIIbβ3-expressing CHO cells stimulated by 100 μg/mL mAb PT25-2 (15 min, 37 °C) in the presence or absence (positive control) of inhibitors: H12, fibrinogen-binding inhibitor dodecapeptide (1 mM) (the total number of contacts, $n = 19\,242$); mAb A2A9, αIIbβ3-specific "antiaggregant" mAb (100 μg/mL) ($n = 24\,661$); cRGD, cyclic RGD peptide (80 μM) ($n = 17\,349$); abciximab (100 μg/mL) ($n = 21\,048$); and tirofiban (100 μM) ($n = 46\,449$). The results are presented as an average from individual cell−bead pairs ± SD.

A2A9 (*20*); a cyclic Arg-Gly-Asp (cRGD) peptide; tirofiban, a tyrosine-based molecule that mimics the three-dimensional structure of RGD (*21*); and abciximab, a murine−human chimeric Fab fragment of the monoclonal antibody 7E3 (*22*). Each produced a substantial decrease in the probability of detecting rupture forces >20 pN (Figure 3), confirming that these rupture forces originate from the interaction of fibrinogen with αIIbβ3.

Next, we measured the effect of increasing concentrations of PT25-2 on the strength of fibrinogen binding to CHO cell αIIbβ3. Because rupture forces <20 pN are nonspecific, they were excluded from the analysis. Further, to derive quantitative parameters for PT25-2-induced fibrinogen binding, the distribution of rupture forces was fitted to the sum of an exponential curve for rupture forces of 20−60 pN and a Gaussian curve for rupture forces >60 pN (eq 1) (*17*). We found that the probability of detecting specific fibrinogen binding to αIIbβ3 increased linearly as the concentration of PT25-2 was increased from 10 to 100 μg/mL (Figure 4 and Table 1). Nonetheless, the average rupture force between the cells and fibrinogen-coated beads, in both the low-to-moderate and strong force regimes, was essentially unchanged. In other words, the probability of detecting specific fibrinogen binding to αIIbβ3 increased as the extent of αIIbβ3 activation increased, but there was no corresponding change in the strength of fibrinogen binding. Further, because PT25-2 binding activates single αIIbβ3 molecules and because the forces measured by laser tweezers are typical for single molecule interactions (*16*, *17*), these results suggest that the two-force regime we detected represents the pathway for fibrinogen binding to single αIIbβ3 molecules.

Interaction of Fibrinogen with CHO Cells Expressing the αIIbβ3 Mutants β3 G708N and αIIb G972N. The β3 mutation G708N and the αIIb mutation G972N induce the binding of soluble FITC-labeled fibrinogen to αIIbβ3 on the surface of transfected CHO cells (*8*, *11*). To study the effects

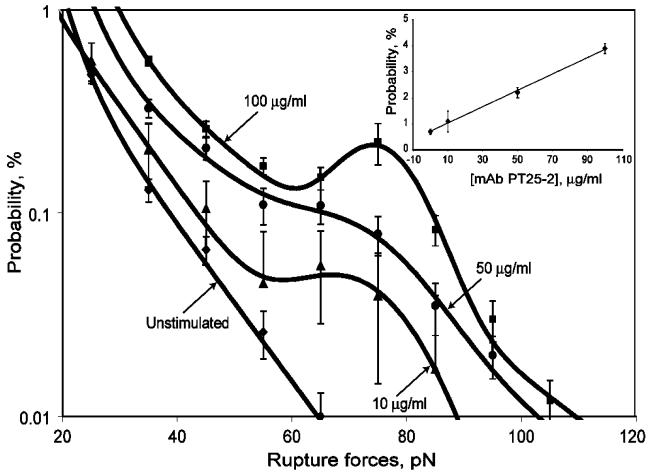

FIGURE 4: Rupture force distributions of the interactions of fibrinogen with the CHO cells expressing WT αIIbβ3 integrin unstimulated or activated by different concentrations of mAb PT25-2. The rupture force profiles are fitted with the sum of an exponential and a Gaussian curve as described by eq 1. Inset: Linear dependence of the cumulative probability of binding interactions >20 pN on the concentration of mAb PT25-2. The cells were pretreated with mAb PT25-2 for 15 min at 37 °C. The total number of contacts (n) included in the histograms was $n = 114\,776$ for unstimulated cells, $n = 22\,610$ for 10 mg/mL mAb, $n = 36\,921$ for 50 mg/mL mAb, and $n = 140\,496$ for 100 mg/mL mAb. Each point of a probability histogram and the linear plot was calculated as an average ± standard deviation from individual files collected from separate cell−bead pairs.

Table 1: Effect of Different Concentrations of the Activating mAb PT25-2 on the Binding Probability and Yield Strength between the WT αIIbβ3-Expressing CHO Cells and Fibrinogen

		yield strength, pN		cumulative probability, %	
CHO cells	N^a	20−60 pN	>60 pN	20−60 pN	>60 pN
no PT25-2	20	30 ± 6	0	0.7 ± 0.1	0
PT25-2 (10 μg/mL)	43	31 ± 5	71 ± 5	1.0 ± 0.4[b]	0.10 ± 0.07[c]
PT25-2 (50 μg/mL)	64	32 ± 6	68 ± 8	1.9 ± 0.2[b]	0.3 ± 0.1[c]
PT25-2 (100 μg/mL)	74	30 ± 7	74 ± 9	3.4 ± 0.2[b]	0.5 ± 0.1[c]

[a] N = the number of cells studied. [b,c] $p < 0.01$, respectively, t-test for unpaired samples.

of these mutations on the function of single αIIbβ3 molecules, we again used laser tweezers. Baseline reactivity of CHO cells expressing either mutant with BSA-coated beads did not differ from CHO cells expressing WT αIIbβ3 and was characterized by weak exponentially decreasing rupture forces, 99.8% of which were <20 pN (not shown). However, there was a striking difference in the rupture force profile when CHO cells expressing the β3 mutant G708N were brought into contact with fibrinogen-coated beads. In the absence of PT25-2, up to 14% of rupture forces were >20 pN (Table 2), and there was a peak of rupture force of >60 pN with a maximum at 75 ± 5 pN (Figure 5). Nonetheless, there were no significant differences in the yield strength of the low-to-moderate and strong force regimes when αIIbβ3 was activated by PT25-2 or β3 G708N (Tables 1 and 2), implying that there was no fundamental difference in the way either form of activated αIIbβ3 interacted with fibrinogen. To confirm that rupture forces >20 pN represented specific fibrinogen binding to αIIbβ3, rupture force measure-

Table 2: Probability and Strength of the Interactions between Fibrinogen and CHO Cells Expressing the β3 G708N αIIbβ3 Mutant in the Absence and Presence of Specific αIIbβ3 and αvβ3 Inhibitors

		yield strength, pN		cumulative probability, %	
	N^a	20−60 pN	>60 pN	20−60 pN	>60 pN
G708N alone	89	31 ± 4	75 ± 5	12.1 ± 1.7	1.9 ± 1.2
G708N + XJ735 (1 mM)	28	29 ± 3	79 ± 7	11.1 ± 1.8[b]	1.0 ± 0.6[c]
G708N + A2A9 (100 μg/mL)	39	29 ± 4	56 ± 19	5.4 ± 0.3[b]	0.20 ± 0.07[c]
G708N + tirofiban (100 μM)	52	29 ± 7	65 ± 15	3.3 ± 0.2[b]	0.11 ± 0.06[c]
G708N + abciximab (100 μg/mL)	19	30 ± 4	indeterminable	1.1 ± 0.2[b]	0.07 ± 0.04[c]

[a] N = the number of cells studied. [b,c] $p < 0.05$, respectively, t-test for unpaired samples.

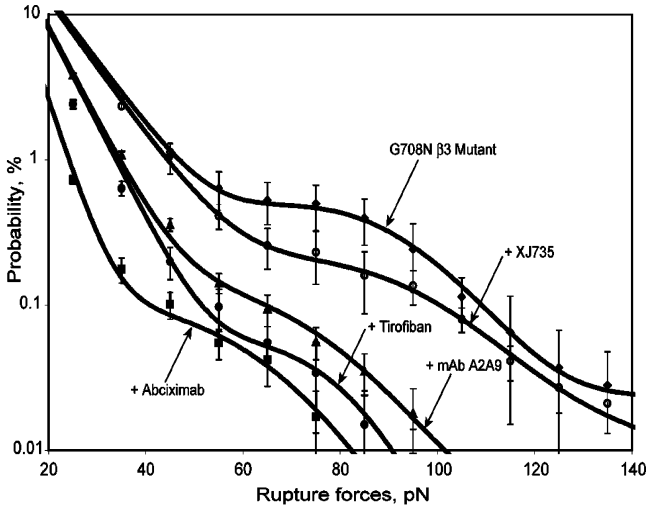

FIGURE 5: Effect of specific αIIbβ3 and αVβ3 inhibitors on the fibrinogen-binding activity of unstimulated CHO cells expressing the β3 G708N αIIbβ3 mutant. The rupture force profiles were fitted with the sum of an exponential and a Gaussian curve as described by eq 1. The total number of contacts (n) included in the histograms was n = 215 002 for the β3 G708N αIIbβ3 mutant without inhibitors, n = 33 892 for XJ735, n = 97 687 for mAb A2A9, n = 128 890 for tirofiban, and n = 22 860 for abciximab. Each point of a probability histogram was calculated as an average ± standard deviation from individual files collected from separate cell−bead pairs.

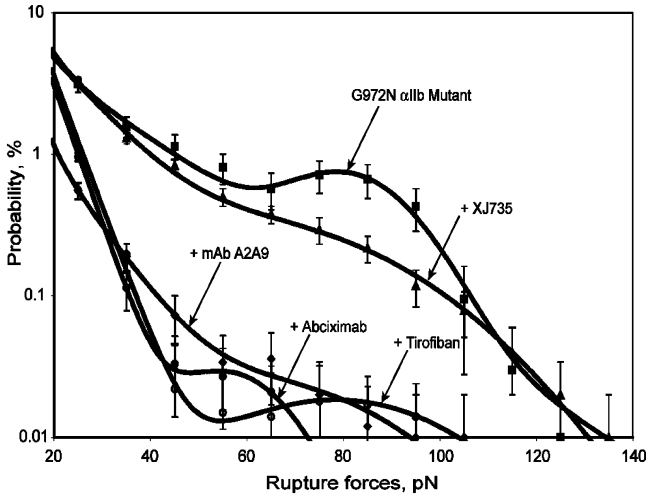

FIGURE 6: Effect of specific αIIbβ3 and αVβ3 inhibitors on the fibrinogen-binding activity of unstimulated CHO cells expressing the αIIb G972N αIIbβ3 mutant. The rupture force profiles were fitted with the sum of an exponential and a Gaussian curve as described by eq 1. The total number of contacts (n) included in the histograms was n = 132 317 for the αIIb G972N αIIbβ3 mutant without inhibitors, n = 38 598 for XJ735, n = 49 548 for mAb A2A9, n = 80 288 for tirofiban, and n = 83 356 for abciximab. Each point of a probability histogram was calculated as an average ± standard deviation from individual files collected from separate cell−bead pairs.

ments were performed in the presence of the αIIbβ3 antagonists abciximab, tirofiban, and A2A9 and the αvβ3 antagonist XJ735 [cyclo(Ala-Arg-Gly-Asp-Mamb); Mamb = *m*-(aminomethyl)benzoic acid], a cyclic RGD-based peptide selective for αvβ3 over αIIbβ3 by 3 orders of magnitude (*23*). Consistent with specific fibrinogen binding to αIIbβ3, the probability of detecting rupture forces of this magnitude was substantially decreased in the presence of the αIIbβ3 antagonists (Figure 5 and Table 2). The values for forces >60 pN in the presence of inhibitors in Table 2 were determined computationally using eq 1 and reflect the positions of centroids of the virtual Gaussian curves that cannot be clearly seen in the corresponding plots shown in Figure 5. XJ735 slightly, but significantly, decreased the cumulative probability of detecting rupture forces >20 pN (Table 2), most likely because it also can bind to αIIbβ3 at higher concentrations. However, CHO cells endogenously express the integrin subunit αv and can form αvβ3 heterodimers when transfected with β3 (*24*). Thus, it is conceivable that β3 G708N could activate αvβ3 as well as αIIbβ3.

In contrast to the β3 mutation G708N, the αIIb mutation G972N decreases the homomeric interaction of peptides corresponding to the αIIb TM helix in the analytical ultracentrifuge (*9*) and when the αIIb TM helix is expressed as a fusion protein in bacterial membranes (*10*). Nonetheless, the profile of rupture forces between fibrinogen-coated beads and CHO cells expressing the αIIbβ3 containing αIIb G972N was essentially the same as that of the β3 G708N-expressing cells. In the absence of PT25-2, up to 11% of rupture forces between fibrinogen-coated beads and G972N-expressing CHO cells were >20 pN, and there were no differences in the yield strength values of the low-to-moderate and strong rupture force regimes between αIIbβ3 containing the αIIb G972N and β3 G708N mutations (Figure 6). Measured rupture forces were specific for fibrinogen binding to αIIbβ3 because they were inhibited by the αIIbβ3 antagonists abciximab, tirofiban, and A2A9 (Figure 6 and Table 3). XJ735 also had a small, but significant, inhibitory effect on both the lower and higher rupture force regimes, consistent with its ability to bind to αIIbβ3 at high concentrations. Thus, these results indicate that perturbing interactions involving either the αIIb or the β3 TM helices of individual αIIbβ3 molecules can shift αIIbβ3 to its high-affinity state and that the interaction of αIIbβ3 with fibrinogen under these conditions is indistinguishable from that of αIIbβ3 in agonist-stimulated platelets (*16*) or following the exposure of αIIbβ3 to Mn^{2+} (*5*, *17*) or mAb PT25-2.

Table 3: Probability and Strength of the Interactions between Fibrinogen and CHO Cells Expressing αIIb G972N Mutant in the Absence and Presence of Specific αIIbβ3 and αvβ3 Inhibitors

		yield strength, pN		cumulative probability, %	
	N^a	20−60 pN	>60 pN	20−60 pN	>60 pN
G972N alone	84	34 ± 5	81 ± 4	6.7 ± 1.9	2.5 ± 1.3
G972N + XJ735 (1 mM)	31	33 ± 4	64 ± 15	5.9 ± 0.7[b]	1.2 ± 0.7[c]
G972N + A2A9 (100 μg/mL)	45	30 ± 5	67 ± 20	0.9 ± 0.3[b]	0.09 ± 0.02[c]
G972N + tirofiban (100 μM)	44	27 ± 6	78 ± 31	0.8 ± 0.2[b]	0.06 ± 0.02[c]
G972N + abciximab (100 μg/mL)	45	28 ± 4	56 ± 10	1.1 ± 0.2[b]	0.02 ± 0.01[c]

[a] N = the number of cells studied. [b,c] $p < 0.05$, respectively, t-test for unpaired samples.

DISCUSSION

By optically trapping and manipulating a small particle using a focused laser beam, external forces applied to the particle can be measured with high resolution in the range of 0−200 pN (*25*, *26*). Using this system, known as laser tweezers, it is possible to obtain details about individual ligand−receptor binding events that might otherwise be missed when conventional receptor−ligand binding studies are performed using large ensembles of molecules or whole cells (*15*). Using laser tweezers, we found that the interaction of fibrinogen with single αIIbβ3 molecules activated by the mAb PT25-2 or by mutation of the αIIb or β3 transmembrane domain had a rupture force profile corresponding to a two-step binding/unbinding pathway that was identical to fibrinogen interaction with αIIbβ3 molecules activated by platelet agonists or the divalent cation Mn^{2+} (*16*, *17*). Thus, our results suggest that the two-step pathway of the integrin−fibrinogen interaction is a fundamental property of the high-affinity state of αIIbβ3.

An alternative possibility is that αIIbβ3 exists in at least two activation states that depend on the nature and/or amount of the integrin-activating stimuli, as has been suggested for several other integrins (*27*−*33*). However, we observed an identical distribution of low-to-moderate and strong rupture forces regardless of whether αIIbβ3 was activated by perturbing its extracellular domain using the mAb PT25-2 or by mutating either the αIIb or β3 TM domains. Moreover, the bimodal distribution of rupture forces induced by mAb PT25-2 was independent of its concentration, and the effect of the αIIb and β3 TM mutations was constitutive, so that, at least under the conditions of these experiments, the pattern of rupture forces we observed cannot be attributed to multiple activation states that result from variations in stimulus intensity.

It was reported previously that fibrinogen binding to purified αIIbβ3 is a time-dependent two-step process in which an initial reversible bond becomes more stable (*34*) and dissociates only in the presence of high concentrations of the tetrapeptide RGDV (*35*). Similarly, Goldsmith et al. reported that the shear-induced breakup of αIIbβ3-coated latex spheres cross-linked by fibrinogen depended on the time of contact between the spheres, suggesting the existence of "young" weak vs "old" strong αIIbβ3−fibrinogen interactions (*36*). A structural basis for these observations is not known, but they are consistent with single molecule studies of the rates of development of weaker and stronger binding interactions (*17*). Naturally occurring and laboratory-induced point mutations that perturb fibrinogen binding to αIIbβ3 map to a "cap subdomain" on the upper surface of αIIb β-propeller (*33*). Thus, it is likely that this region of the αIIbβ3 molecule interacts most extensively with the carboxyl terminus of the fibrinogen γ-chain. Nonetheless, it has been reported that the cap subdomain does not undergo allosteric changes during αIIbβ3 activation or following ligand binding (*33*). Accordingly, it is possible that the stronger interaction of fibrinogen with αIIbβ3 occurs when, after initial contact, other regions of either αIIbβ3 and/or fibrinogen interact.

There is compelling evidence that TM domain interactions are involved in integrin regulation. Using flow cytometry to measure fibrinogen binding to recombinant αIIbβ3 expressed by CHO cells, we reported that mutation of αIIb TM domain residues G972 and G976 or β3 TM domain residues M701 and G708 induced constitutive αIIbβ3 activity (*8*, *11*). Luo et al. expressed αIIb and β3 TM helix mutants in both CHO and 293T cells (*13*), confirming that mutating αIIb residues G972 and G976 induced constitutive αIIbβ3 activity and that mutating residue T981 activated the integrin as well. They also observed that mutating β3 residue G708 induced αIIbβ3 activation in CHO, but not 293T, cells. Partridge et al. (*37*) used random mutagenesis of the β3 TM and cytoplasmic domains to search for interactions constraining αIIbβ3 activation. They detected 13 activating mutations in the β3 TM helix, 9 of which were predicted to shorten the helix. The 4 remaining mutations, including a G708S mutation, were located in carboxyl-terminal half of the helix and were postulated to activate αIIbβ3 by disrupting the packing of an αIIb/β3 TM heterodimer. We also observed that the αIIbβ3 activation induced by TM domain mutations was accompanied by redistribution of αIIbβ3 on the CHO cell surface, consistent with the formation of αIIbβ3 clusters (*8*, *11*). However, Luo et al. (*13*) were unable to detect αIIbβ3 macroclusters on the surface of CHO cells expressing the β3 G708N mutant. It is noteworthy that the activating effect of the β3 G708N mutant they reported in CHO cells was relatively small. We have observed that the effect of this mutation is directly proportional to the level of αIIbβ3 expression (*8*). Since one would predict that the formation of αIIbβ3 clusters is directly related to the density of activated integrin in the cell membrane, it is possible that their inability to observe clusters might be due to a relatively low level of αIIbβ3 expression.

Our laser tweezers-based model system was designed to measure single-molecule interactions (*17*, *38*) and therefore cannot address the role of clustering in regulating αIIbβ3 activity. Nonetheless, we have not detected differences between the bimodal activation pathway of isolated immobilized αIIbβ3 molecules, where clustering is not possible (*17*), and αIIbβ3 molecules on the surface of platelets and CHO cells. Thus, if αIIbβ3 clustering does occur on cell surfaces, our results suggest that it does not have a detectable

effect on the interaction between individual αIIbβ3 and fibrinogen molecules. On the other hand, the physical basis for the presence of a bimodal distribution of rupture forces we observe is not known. However, we reported previously that the strong force component was relatively labile, decreasing as a function of the time of storage of purified αIIbβ3 at 4 °C, and, importantly, was directly proportional to the duration of contact between fibrinogen and αIIbβ3 (*17*), the latter suggesting that there may be rearrangement of the αIIbβ3 ligand binding domain following its initial interaction with fibrinogen. Nonetheless, our data indicate that αIIbβ3 appears to undergo an allosteric switch between inactive and fully active states in which the function of activating stimuli is to alter the proportion of molecules in inactive and active conformations. Thus, the propensity of a TM domain mutation, for example, to induce constitutive αIIbβ3 activity, is related to its propensity to disrupt or enhance TM domain associations.

Our ability to specifically attribute measured rupture forces to fibrinogen bound to activated αIIbβ3 is based on the ability of known αIIbβ3 antagonists to abrogate these forces. It is noteworthy in this regard that 1 mM XJ735, an αvβ3-specific cyclic peptide, had a small, but significant, effect on the interaction of fibrinogen-coated beads with CHO cells expressing either β3 G708N or αIIb G972N. However, we noted previously that this concentration of XJ735 had a substantial inhibitory effect on the adhesion of ADP-stimulated platelets to fibrinogen-coated surfaces (*39*). Thus, it is likely that cross-reactivity accounts for the ability of XJ735 to inhibit fibrinogen binding to the αIIbβ3 TM domain mutants.

Although it is tempting to apply Bell's function (*40*, *41*) to fit the force distribution we have measured in order to obtain thermodynamic and kinetic binding parameters, there are several limitations of our data that preclude such an analysis. First, as we have shown previously (*17*), integrin−fibrinogen binding strength does not depend on the loading rate, which contradicts the standard theory. Second, the lower part of the rupture force spectrum likely represents a combination of specific, as well as nonspecific, cell−protein interactions, as judged from Figures 2 and 4−6. In addition, there are other potential reasons for a failure of a simple model for unbinding (*42*−*44*) that are beyond the scope of the present work.

In conclusion, using laser tweezer-based force spectroscopy and transfected CHO cells, we found that the interaction of fibrinogen with single αIIbβ3 molecules activated by the mAb PT25-2 or either of two αIIbβ3 TM domain mutations had a rupture force profile corresponding to a two-step binding/unbinding pathway that was identical to the interaction of fibrinogen with αIIbβ3 on agonist-stimulated platelets (*16*) or purified and immobilized αIIbβ3 molecules incubated with a millimolar concentration of Mn^{2+} (*17*). Thus, the two-step pathway of the integrin−fibrinogen interaction appears to be a fundamental property of the high-affinity state of αIIbβ3 and is identical regardless of whether this affinity state is achieved by intracellular, extracellular, or membrane-associated events.

ACKNOWLEDGMENT

We are very grateful to Dr. Henry Shuman (Department of Physiology, University of Pennsylvania School of Medicine) for the construction of our optical trap instrumentation, for fruitful discussions of physical principles of single-molecule unbinding experiments, and for software used in data analysis.

NOTE ADDED AFTER ASAP PUBLICATION

This paper was published prematurely March 28, 2006. The last sentence of the legend of Figure 1 was changed to include the word "not". The correct version of this paper was published March 31, 2006.

REFERENCES

1. Bennett, J. S. (1996) Structural biology of glycoprotein IIb-IIIa, *Trends Cardiovasc. Med. 16*, 31−36.
2. Arnaout, M. A., Goodman, S. L., and Xiong, J. P. (2002) Coming to grips with integrin binding to ligands, *Curr. Opin. Cell Biol. 14*, 641−651.
3. Springer, T. A., and Wang, J. H. (2004) The three-dimensional structure of integrins and their ligands, and conformational regulation of cell adhesion, *Adv. Protein Chem. 68*, 29−63.
4. Ginsberg, M. H., Lightsey, A., Kunicki, T. J., Kaufmann, A., Marguerie, G., and Plow, E. F. (1986) Divalent cation regulation of the surface orientation of platelet membrane glycoprotein IIb. Correlation with fibrinogen binding function and definition of a novel variant of Glanzmann's thrombasthenia, *J. Clin. Invest. 78*, 1103−1111.
5. Litvinov, R. I., Nagaswami, C., Vilaire, G., Shuman, H., Bennett, J. S., and Weisel, J. W. (2004) Functional and structural correlations of individual alphaIIbbeta3 molecules, *Blood 104*, 3979−3985.
6. Kim, M., Carman, C. V., and Springer, T. A. (2003) Bidirectional transmembrane signaling by cytoplasmic domain separation in integrins, *Science 301*, 1720−1725.
7. Fox, J. E., Shattil, S. J., Kinlough-Rathbone, R. L., Richardson, M., Packham, M. A., and Sanan, D. A. (1996) The platelet cytoskeleton stabilizes the interaction between alphaIIbbeta3 and its ligand and induces selective movements of ligand-occupied integrin, *J. Biol. Chem. 271*, 7004−7011.
8. Li, R., Mitra, N., Gratkowski, H., Vilaire, G., Litvinov, R., Nagasami, C., Weisel, J. W., Lear, J. D., DeGrado, W. F., and Bennett, J. S. (2003) Activation of integrin alphaIIbbeta3 by modulation of transmembrane helix associations, *Science 300*, 795−798.
9. Li, R., Babu, C. R., Lear, J. D., Wand, A. J., Bennett, J. S., and DeGrado, W. F. (2001) Oligomerization of the integrin alphaI-Ibbeta3: roles of the transmembrane and cytoplasmic domains, *Proc. Natl. Acad. Sci. U.S.A. 98*, 12462−12467.
10. Li, R., Gorelik, R., Nanda, V., Law, P. B., Lear, J. D., DeGrado, W. F., and Bennett, J. S. (2004) Dimerization of the transmembrane domain of integrin alphaIIb subunit in cell membranes, *J. Biol. Chem. 279*, 26666−26673.
11. Li, W., Metcalf, D. G., Gorelik, R., Li, R., Mitra, N., Nanda, V., Law, P. B., Lear, J. D., DeGrado, W. F., and Bennett, J. S. (2005) A push−pull mechanism for regulating integrin function, *Proc. Natl. Acad. Sci. U.S.A. 102*, 1424−1429.
12. Luo, B. H., Springer, T. A., and Takagi, J. (2004) A specific interface between integrin transmembrane helices and affinity for ligand, *PLoS Biol. 2*, e153.
13. Luo, B. H., Carman, C. V., Takagi, J., and Springer, T. A. (2005) Disrupting integrin transmembrane domain heterodimerization increases ligand binding affinity, not valency or clustering, *Proc. Natl. Acad. Sci. U.S.A. 102*, 3679−3684.
14. Visscher, K., and Block, S. M. (1998) Versatile optical traps with feedback control, *Methods Enzymol. 298*, 460−489.
15. Weisel, J. W., Shuman, H., and Litvinov, R. I. (2003) Protein−protein unbinding induced by force: single-molecule studies, *Curr. Opin. Struct. Biol. 13*, 227−235.
16. Litvinov, R. I., Shuman, H., Bennett, J. S., and Weisel, J. W. (2002) Binding strength and activation state of single fibrinogen-integrin pairs on living cells, *Proc. Natl. Acad. Sci. U.S.A. 99*, 7426−7431.
17. Litvinov, R. I., Bennett, J. S., Weisel, J. W., and Shuman, H. (2005) Multi-step fibrinogen binding to the integrin {alpha}IIb{beta}3 detected using force spectroscopy, *Biophys. J. 89*, 2824−2834.

18. Tokuhira, M., Handa, M., Kamata, T., Oda, A., Katayama, M., Tomiyama, Y., Murata, M., Kawai, Y., Watanabe, K., and Ikeda, Y. (1996) A novel regulatory epitope defined by a murine monoclonal antibody to the platelet GPIIb-IIIa complex (alpha IIb beta 3 integrin), *Thromb. Haemostasis 76*, 1038−1046.
19. Kloczwiak, M., Timmons, S., Lukas, T. J., and Hawiger, J. (1984) Platelet receptor recognition site on human fibrinogen. Synthesis and structure−function relationship of peptides corresponding to the carboxy-terminal segment of the gamma chain, *Biochemistry 23*, 1767−1774.
20. Bennett, J. S., Hoxie, J. A., Leitman, S. F., Vilaire, G., and Cines, D. B. (1983) Inhibition of fibrinogen binding to stimulated human platelets by a monoclonal antibody, *Proc. Natl. Acad. Sci. U.S.A. 80*, 2417−2421.
21. Cook, J. J., Bednar, B., J. L. Lynch, J., Gould, R. J., Egberson, M. S., Halczenko, W., Duggan, M. E., Hartman, G. D., Lo, M.-W., Murphy, G. M., Deckelbaum, L. I., Sax, F. L., and Barr, E. (1999) Tirofiban (Aggrastat M), *Cardiovasc. Drug Rev. 17*, 199−224.
22. Coller, B. S. (1985) A new murine monoclonal antibody reports an activation-dependent change in the conformation and/or microenvironment of the platelet glycoprotein IIb/IIIa complex, *J. Clin. Invest. 76*, 101−108.
23. Bach, A. C., Espina, J. R., Jackson, S. A., Stouten, P. F. W., Duke, J. L., Mousa, S. A., and DeGrado, W. F. (1996) Type II′ to type I β-turn swap changes specificity for integrins, *J. Am. Chem. Soc. 118*, 293−294.
24. Zaffran, Y., Meyer, S. C., Negrescu, E., Reddy, K. B., and Fox, J. E. (2000) Signaling across the platelet adhesion receptor glycoprotein Ib-IX induces alpha IIbbeta 3 activation both in platelets and a transfected Chinese hamster ovary cell system, *J. Biol. Chem. 275*, 16779−16787.
25. Simmons, R. M., Finer, J. T., Chu, S., and Spudich, J. A. (1996) Quantitative measurements of force and displacement using an optical trap, *Biophys. J. 70*, 1813−1822.
26. Brouhard, G. J., Schek, H. T., III, and Hunt, A. J. (2003) Advanced optical tweezers for the study of cellular and molecular biomechanics, *IEEE Trans. Biomed. Eng. 50*, 121−125.
27. Garcia, A. J., Takagi, J., and Boettiger, D. (1998) Two-stage activation for alpha5beta1 integrin binding to surface-adsorbed fibronectin, *J. Biol. Chem. 273*, 34710−34715.
28. Boettiger, D., Huber, F., Lynch, L., and Blystone, S. (2001) Activation of alpha(v)beta3-vitronectin binding is a multistage process in which increases in bond strength are dependent on Y747 and Y759 in the cytoplasmic domain of beta3, *Mol. Biol. Cell 12*, 1227−1237.
29. Garcia, A. J., Schwarzbauer, J. E., and Boettiger, D. (2002) Distinct activation states of alpha5beta1 integrin show differential binding to RGD and synergy domains of fibronectin, *Biochemistry 41*, 9063−9069.
30. Chigaev, A., Blenc, A. M., Braaten, J. V., Kumaraswamy, N., Kepley, C. L., Andrews, R. P., Oliver, J. M., Edwards, B. S., Prossnitz, E. R., Larson, R. S., and Sklar, L. A. (2001) Real time analysis of the affinity regulation of alpha 4-integrin. The physiologically activated receptor is intermediate in affinity between resting and Mn(2+) or antibody activation, *J. Biol. Chem. 276*, 48670−48678.
31. Chigaev, A., Zwartz, G. J., Buranda, T., Edwards, B. S., Prossnitz, E. R., and Sklar, L. A. (2004) Conformational regulation of {alpha}4{beta}1-integrin affinity by reducing agents: inside-out signaling is independent of an additive to rediction-regulated integrin activation, *J. Biol. Chem. 279*, 32435−32443.
32. Pampori, N., Hato, T., Stupack, D. G., Aidoudi, S., Cheresh, D. A., Nemerow, G. R., and Shattil, S. J. (1999) Mechanisms and consequences of affinity modulation of integrin alpha(V)beta(3) detected with a novel patch-engineered monovalent ligand, *J. Biol. Chem. 274*, 21609−21616.
33. Xiao, T., Takagi, J., Coller, B. S., Wang, J. H., and Springer, T. A. (2004) Structural basis for allostery in integrins and binding to fibrinogen-mimetic therapeutics, *Nature 432*, 59−67.
34. Muller, B., Zerwes, H. G., Tangemann, K., Peter, J., and Engel, J. (1993) Two-step binding mechanism of fibrinogen to alpha IIb beta 3 integrin reconstituted into planar lipid bilayers, *J. Biol. Chem. 268*, 6800−6808.
35. Huber, W., Hurst, J., Schlatter, D., Barner, R., Hubscher, J., Kouns, W. C., and Steiner, B. (1995) Determination of kinetic constants for the interaction between the platelet glycoprotein IIb-IIIa and fibrinogen by means of surface plasmon resonance, *Eur. J. Biochem. 227*, 647−656.
36. Goldsmith, H. L., McIntosh, F. A., Shahin, J., and Frojmovic, M. M. (2000) Time and force dependence of the rupture of glycoprotein IIb-IIIa-fibrinogen bonds between latex spheres, *Biophys. J. 78*, 1195−1206.
37. Partridge, A. W., Liu, S., Kim, S., Bowie, J. U., and Ginsberg, M. H. (2005) Transmembrane domain helix packing stabilizes integrin {alpha}IIb{beta}3 in the low affinity state, *J. Biol. Chem. 280*, 7294−7300.
38. Liphardt, J., Dumont, S., Smith, S. B., Tinoco, I., Jr., and Bustamante, C. (2002) Equilibrium information from nonequilibrium measurements in an experimental test of Jarzynski's equality, *Science 296*, 1832−1835.
39. Bennett, J. S., Chan, C., Vilaire, G., Mousa, S. A., and DeGrado, W. F. (1997) Agonist-activated alphavbeta3 on platelets and lymphocytes binds to the matrix protein osteopontin, *J. Biol. Chem. 272*, 8137−8140.
40. Bell, G. I. (1978) Models for the specific adhesion of cells to cells, *Science 200*, 618−627.
41. Evans, E., and Ritchie, K. (1997) Dynamic strength of molecular adhesion bonds, *Biophys. J. 72*, 1541−1555.
42. Bartolo, D., Derenyi, I., and Ajdari, A. (2002) Dynamic response of adhesion complexes: beyond the single-path picture, *Phys. Rev. E: Stat., Nonlinear, Soft Matter Phys. 65*, 051910.
43. Dudko, O. K., Filippov, A. E., Klafter, J., and Urbakh, M. (2003) Beyond the conventional description of dynamic force spectroscopy of adhesion bonds, *Proc. Natl. Acad. Sci. U.S.A. 100*, 11378−11381.
44. Derenyi, I., Bartolo, D., and Ajdari, A. (2004) Effects of intermediate bound states in dynamic force spectroscopy, *Biophys. J. 86*, 1263−1269.

BI0526581